Journal of Power Sources 215 (2012) 233–239

Contents lists available at SciVerse ScienceDirect

Journal of Power Sources

journal homepage: www.elsevier.com/locate/jpowsour

Platinum oxidation responsible for degradation of platinum–cobalt alloy cathode catalysts for polymer electrolyte fuel cells

Shoichi Hidai [a,b,*], Masaki Kobayashi [a,c], Hideharu Niwa [a], Yoshihisa Harada [a,c], Masaharu Oshima [a,c], Yoji Nakamori [b], Tsutomu Aoki [b]

[a] Department of Applied Chemistry, School of Engineering, The University of Tokyo, Hongo, Bunkyo-ku, Tokyo 113-8656, Japan
[b] Toshiba Fuel Cell Power Systems Corporation, Ukishima-cho, Kawasaki-ku, Kawasaki-shi, Kanagawa 210-0862, Japan
[c] Synchrotron Radiation Research Organization, The University of Tokyo, Hongo, Bunkyo-ku, Tokyo 113-8656, Japan

HIGHLIGHTS

- Large particles and hot annealing improves Pt–Co alloy catalyst durability.
- The Pt 4*f* XPS spectra suggests that high $Pt(OH)_2$ contents increase Pt dissolution.
- Applying the potential step of 1.2 V, Pt oxides, PtO and PtO_2, were produced.
- Pt–Co alloy catalyst durability can be improved by preventing Pt oxidization.

ARTICLE INFO

Article history:
Received 27 January 2012
Received in revised form
28 April 2012
Accepted 1 May 2012
Available online 16 May 2012

Keywords:
Polymer electrolyte fuel cell
Cathode catalyst
Pt–Co alloy
Soft X-ray photoemission spectroscopy
Platinum oxides
Catalyst durability

ABSTRACT

Platinum oxidation of Pt–Co alloy catalysts for polymer electrolyte fuel cells was investigated for a series of Pt–Co alloy catalysts with different specification. The chemical state of platinum evaluated by soft X-ray photoemission spectroscopy was compared with the electrochemical properties to elucidate the origin of catalyst degradation. Increase in the particle size of Pt–Co alloy catalysts caused the decrease in the concentration of platinum hydroxide and improved the catalyst durability. Applying potential cycling below 1.0 V, only platinum hydroxide was observed, while platinum oxides, PtO and PtO_2, appeared after potential cycling up to 1.2 V. The peak shift of Pt 4*f* spectra after the potential cycling implies that these platinum hydroxide and oxide are dissolved and deposited on another platinum catalyst in a reduced metallic state, which causes the catalyst degradation.

1. Introduction

Polymer electrolyte fuel cell (PEFC) is developed as a clean and high efficiency energy source for stationary, auto mobile, mobile applications. Platinum nano-particles loaded on carbon support are used as conventional PEFC cathode catalysts for oxygen reduction reaction. For commercialization of the PEFC system, it is necessary to decrease the amount of platinum loading because platinum is an expensive and rare material [1]. Platinum alloyed with a first row transition metal is one of the most promising candidate materials due to its higher catalytic activity than the pure platinum catalyst [2–4]. In particular, Pt–Ni and Pt–Co alloys have been reported to show the highest activity among the Pt alloy catalysts [2,3]. High durability of Pt alloy catalysts is another important requisite for commercialization of the PEFC system. In conventional platinum nano-particle catalysts, the growth of the particle size decreases the active area and cell performance [5]. Dissolved platinum ions from nano-particles may deposit on other platinum particles, leading to the increase in the particle size, named Ostwald's ripening [6,7]. Mitsushima et al. [8] have suggested that the platinum dissolution is accelerated by potential cycling, and that platinum oxidation and reduction should be responsible for the platinum dissolution. There have been some reports on the durability of Pt alloy catalysts [9,10]. The Pt–Co alloy catalyst shows higher durability than the platinum nano-particle catalyst both in accelerating testing and under PEFC operation. Matsutani et al. [11] have studied the particle size effect on the stability of cell

* Corresponding author. Toshiba Fuel Cell Power Systems Corporation, Ukishima-cho, Kawasaki-ku, Kawasaki-shi, Kanagawa 210-0862, Japan. Tel.: +81 44 288 8021; fax: +81 44 288 8212.
E-mail addresses: shoichi.hidai@toshiba.co.jp, hidai@sr.t.u-tokyo.ac.jp (S. Hidai).

0378-7753/$ – see front matter © 2012 Elsevier B.V. All rights reserved.
doi:10.1016/j.jpowsour.2012.05.001

Table 1
Loading conditions, annealing temperature, and particle size before and after potential cycling between 0.6 V and 1.0 V of Pt–Co alloy catalysts.

Sample name	Pt loading (wt%)	Co loading (wt%)	Annealing temperature	Initial particle size (nm)	Particle size after potential cycling (nm)
A: 47L	46.9	5.2	900 °C [11]	6.1	5.9
B: 28L	28.3	2.4	900 °C [11]	4.1	5.2
C: 47H	47.0	4.3	Higher than 1000 °C [11]	7.5	7.0
D: 28H	28.1	3.9	Higher than 1000 °C [11]	5.8	5.4

performance for platinum and Pt–Co alloy catalysts and have found that irrespective of catalyst type, large particle catalysts are stable. We compared Pt 4*f* states of Pt–Co alloy catalysts with Pt nano-particle catalysts [12] and concluded that platinum oxidation induces large degradation of Pt nano-particle catalysts. However, the mechanism for the high durability of the Pt–Co alloy catalyst is not clear yet.

In this study, we have investigated the origin of degradation of the Pt–Co alloy catalysts. To investigate the Pt–Co alloy catalyst degradation precisely, we have investigated platinum oxidation of Pt–Co alloy catalyst by monitoring Pt 4*f* core levels of Pt–Co alloy catalysts with different particle size in membrane electrode assembly (MEA) before and after potential cycling at different upper potential during potential cycling.

2. Experimental

We have investigated four types of Pt–Co alloy catalyst powders with different catalyst loading and annealing temperature made by Tanaka Kikinzoku Kogyo as listed in Table 1. The Pt–Co alloy particles were loaded on high surface area carbon, annealed and then rinsed by nitric acid [11]. We denote here the catalysts by platinum loading percentage and annealing temperature. For example, the catalyst A 47L means 47% of platinum loading and low annealing temperature. The catalyst powder was mixed with a perfluoro-sulfonate ionomer solution, Aciplex SS (made by Asahi Kasei) to produce a catalyst ink. The ink was then spread and dried on a support film to make a decal sheet. A pair of the decal sheets was hot-pressed on an electrolyte membrane to make an MEA. A pair of non-woven carbon sheets covered with a micro porous layer was attached on both sides of the MEA as gas diffusion layers (GDL). Potential cycling was applied to MEA on the following conditions. Cell temperature was maintained at 80 °C by external heaters. Fully humidified hydrogen was introduced to the anode and fully humidified nitrogen to the cathode. Square-shaped potential waves were applied to the cell by 10,000 cycles. The potential was kept at lower potential for 3 s and upper potential for another 3 s in one cycle. The lower potential was 0.6 V and the upper potential was 1.0 V. The potential condition was selected to minimize the carbon corrosion which might be significant over 1.0 V [13,14]. In order to evaluate the upper potential effect, we also conducted the potential cycle between 0.6 V and 1.2 V. Electrochemical surface area (ECA) of the samples was evaluated as indicator of catalyst degradation. ECA was calculated by integrating hydrogen adsorption charge in cyclic voltammogram (CV) measurements and dividing it by 0.21 mC cm^{-2} [15]. The CV measurements were conducted at cell temperature of 30 °C, where fully humidified hydrogen and nitrogen were introduced to the anode and the cathode, respectively. The potential was applied from 0.05 V to 1.0 V with a sweep rate of 10 mV s^{-1}, regulated using an electrochemical measurement system (HZ5000, Hokuto Denko). To evaluate the catalyst particle size and the structural change of the catalyst layer, transmission electron microscopy (TEM) images were obtained using transmission electron microscope (H-7100FA, Hitachi) operated at an acceleration voltage of 100 kV. Soft X-ray photoemission spectroscopy (SXPES) measurements were conducted on initial MEA and cycle-tested MEA at BL27SU of SPring-8. For MEA samples, GDLs were removed and X-rays were irradiated on the GDL side of the cathode catalyst layer. Incident photon energy was set at 1 keV with the energy resolution of 200 meV. The measurements were conducted in an ultra-high vacuum below 4×10^{-8} Pa at room temperature. Binding energies were calibrated by the peak energy of the Au 4*f* line. The probing depth of the SXPES photoelectrons was approximately 3.4 nm at the Pt 4*f* line.

3. Results and discussion

3.1. Change of chemical states of platinum of Pt–Co alloy catalysts

Four types of Pt–Co alloy catalysts from A to D listed in Table 1 were evaluated in terms of their durability against potential cycling between 0.6 V and 1.0 V for 10,000 cycles. The mean particle sizes of initial catalysts are 6.1, 4.1, 7.5 and 5.8 nm, respectively as listed in Table 1. The ECAs during the potential cycling are compared in Fig. 1. The ECA of the catalysts A 47L, B 28L and D 28H decreased, suggesting that the catalysts were degraded by the potential cycling. Platinum dissolution might cause the ECA decay in those catalysts analogous to Pt nano-particle catalysts. TEM images of all MEA samples at the interface between the membrane (upper side of the pictures) and the cathode are shown in Fig. 2. The large grain of Pt can be observed at the interface between the catalyst layer and the membrane of the cycle-tested MEAs. Part of the dissolved platinum from the catalysts deposited to make the large grain. This platinum deposition is apart from the carbon support and isn't included in the ECA. Therefore after the potential cycling the ECA of catalysts A 47L, B 28L and D 28H decreased with decreasing the amount of the active Pt. The particle sizes distributions, measured from the TEM images, are shown in Fig. S1 of the supporting material. The mean values of the particle size after the potential cycling are compared in Table 1. Pt dissolution may also decrease the particle size of the

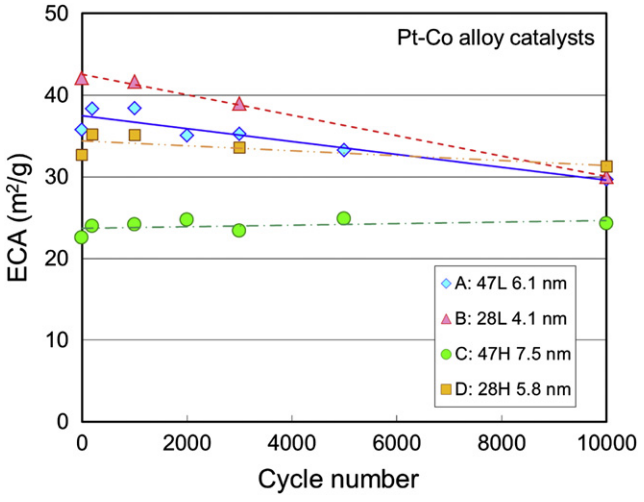

Fig. 1. The comparison of ECA decay on Pt–Co catalysts during potential cycling.

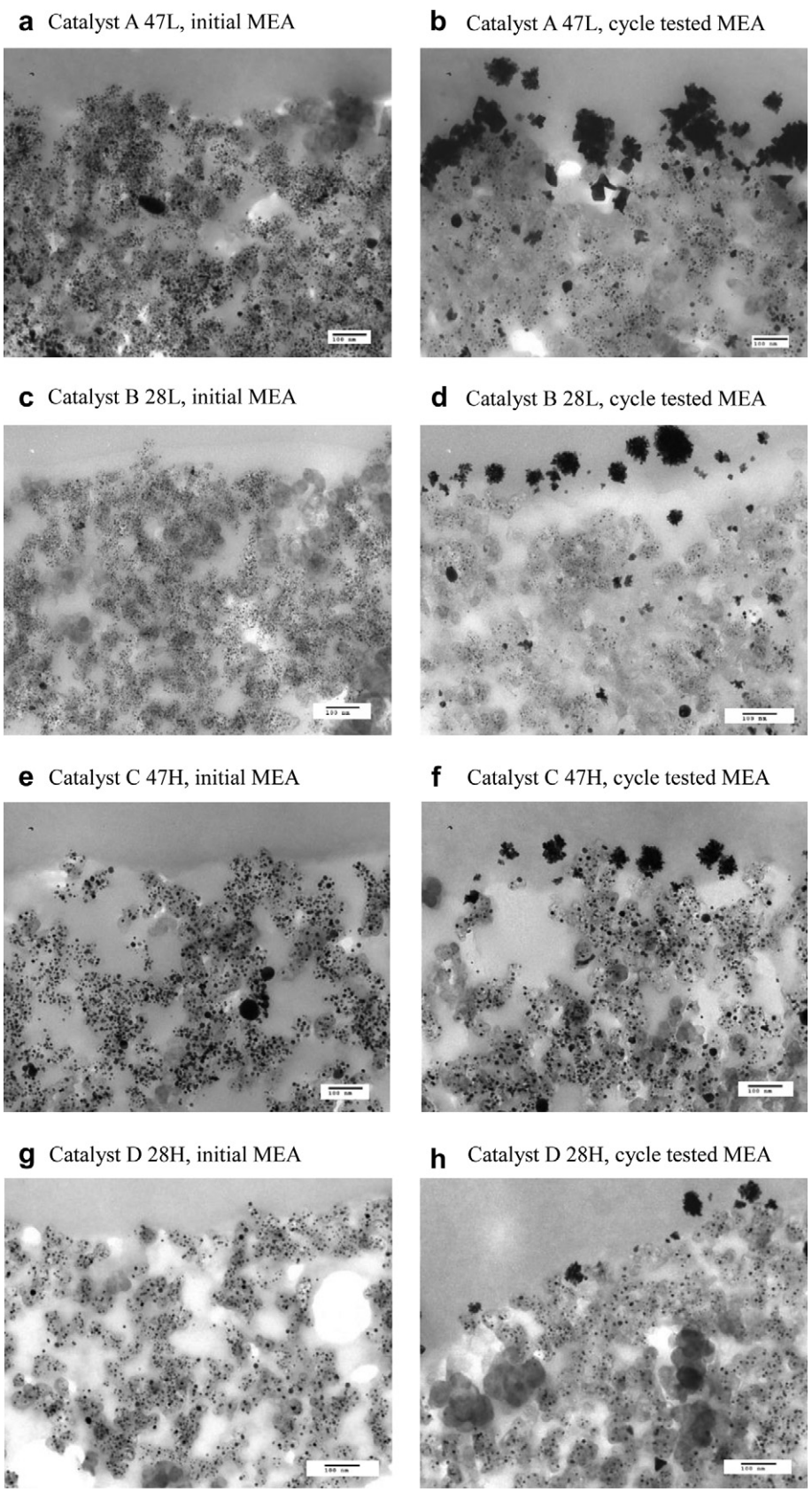

Fig. 2. TEM images at the interface between the electrolyte membrane (upper side) and the cathode catalyst layer of (a) initial MEA of catalyst A 47L, (b) cycle-tested MEA of catalyst A 47L, (c) initial MEA of catalyst B 28L, (d) cycle-tested MEA of catalyst B 28L, (e) initial MEA of catalyst C 47H, (f) cycle-tested MEA of catalyst C 47H, (g) initial MEA of catalyst D 28H and (h) cycle-tested MEA of catalyst D 28H.

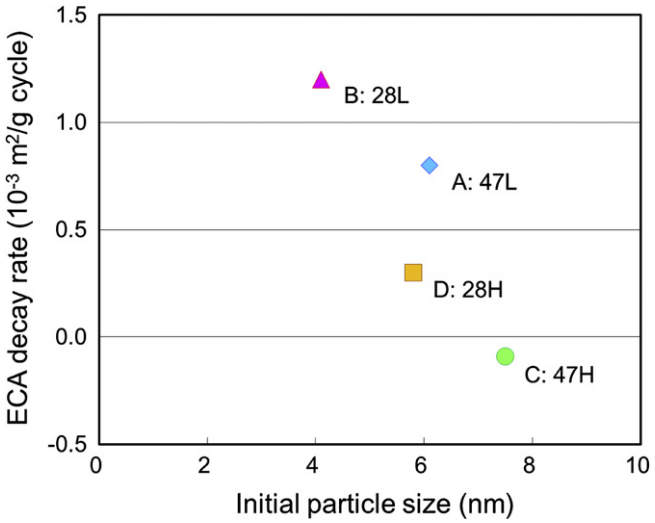

Fig. 3. The relationship between initial particle sizes and ECA decay rates.

catalysts. This is applicable to the catalysts A 47L and D 28H. However, the particle size of the catalyst B 28L, which has the smallest initial particle size, was increased against expectations from the largest ECA decay of the catalyst B 28L among the catalysts. It is possibly due to deposition of a part of the dissolved platinum atoms on other catalyst particles in the catalyst B 28L through the Ostwald's ripening process [6,7]. In contrast, for the catalyst C 47H showing a constant ECA the particle size was decreased. In this case, the decrease of the particle size does not seem to influence the ECA. The changes in the distribution of the particle size are shown in Fig. S1 of the supporting material. The particles with the diameter of about 10 nm decreased in the catalyst

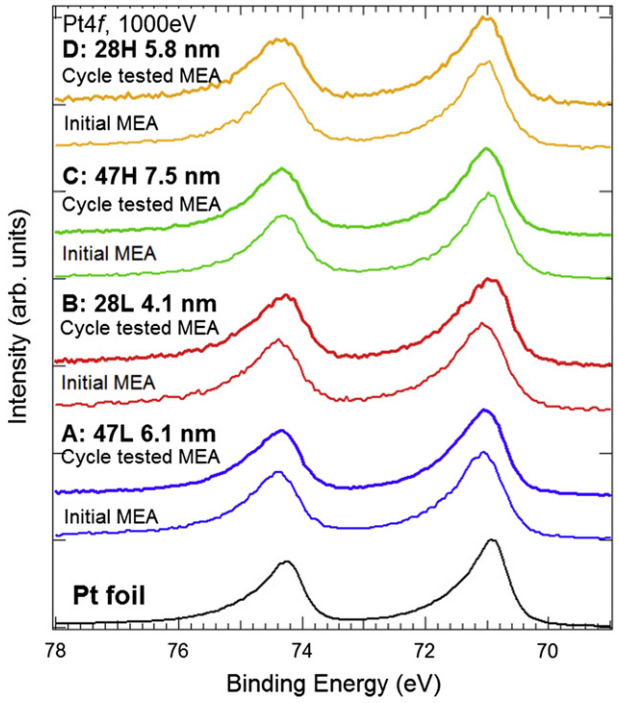

Fig. 4. Pt 4*f* core-level SXPES spectra for all the catalysts under initial MEA and cycle-tested MEA conditions together with a reference Pf foil. Thin lines are initial MEA and solid lines are cycle-tested MEA.

Table 2
Composition ratios of chemical states in initial MEA and cycle-tested MEA determined from SXPES measurements (%).

		Pt^0	PtO_{ads}	$Pt(OH)_2$	PtO	PtO_2
Peak shift from Pt^0 (eV)		0	0.9 [17,22]	1.4 [18]	2.6 [17,21]	4.4 [17]
A: 47L	Initial	86	12	2	1	0
	Cycle-tested	87	13	0	0	0
B: 28L	Initial	91	5	5	0	0
	Cycle-tested	91	6	2	0	0
C: 47H	Initial	88	12	0	0	0
	Cycle-tested	92	6	2	0	0
D: 28H	Initial	90	7	3	1	0
	Cycle-tested	84	13	1	2	0

C 47H after the potential cycling. It is possible that these large size particles are divided into smaller particles by the potential cycling, which may effectively compensate the decrease of the ECA by Pt dissolution.

The ECAs of all the samples during potential cycling in Fig. 1 linearly decrease. In order to compare the degradation rates of the catalysts, we determined the ECA decay rates as the slope of linear fitting lines. The decay rates of all the catalysts as a function of the initial particle size are shown in Fig. 3. It is found that the ECA decay rate decreases with the increase of the initial particle size. The initial particle size is inversely proportional to the ECA of the catalyst in MEAs when the applied platinum weights are identical [supporting material], while ECA decreases with the platinum dissolution since the platinum dissolves from the surface. Taking all these considerations into account, we can conclude from the results of Fig. 3 that the larger the particle size is, the more slowly the platinum dissolution occurs.

The ECA decay rates of the catalysts shown in Fig. 3 can be categorized by annealing temperature. From the results on the catalyst C 47H and D 28H, it is revealed that high annealing temperature suppresses the ECA decay during potential cycling. This result seems to be consistent with TEM images in Fig. 2, as the Pt deposition of the catalyst C 47H and D 28H are smaller and less than those of the catalyst A 47L and B 28L. For platinum and transition metal alloy catalysts, it is reported that the surface of the annealed catalyst is covered with pure platinum, i.e. Pt skin layer, formed by surface segregation occurring during the annealing [3,4].

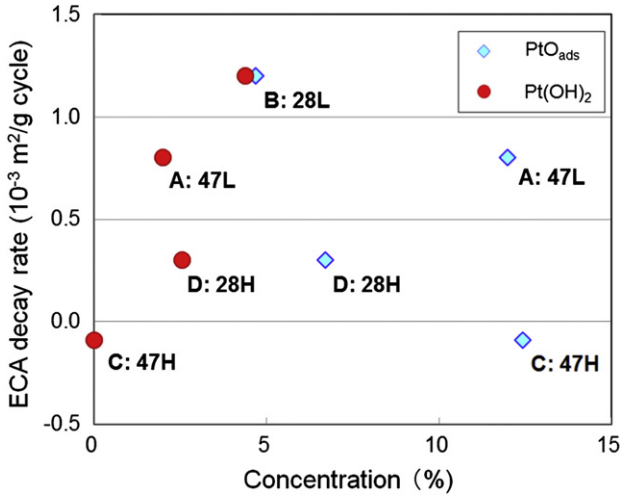

Fig. 5. Platinum hydroxide and oxygen adsorption concentration effect on ECA decay rate. Diamond and circle symbols indicate oxygen adsorbed platinum component and platinum hydroxide component, respectively.

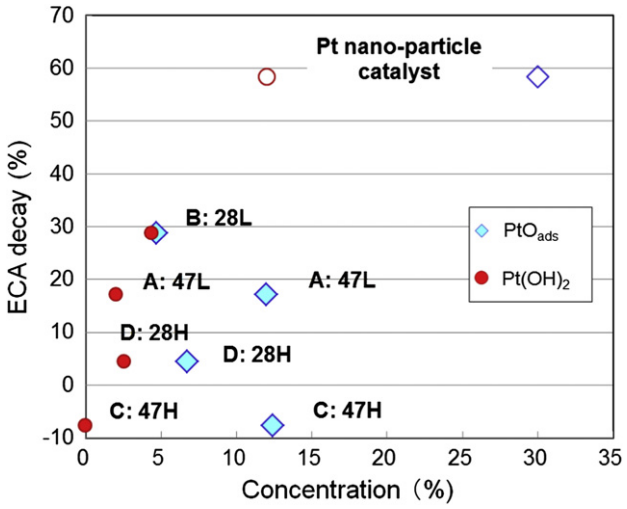

Fig. 6. ECA decay ratio after potential cycling against the platinum hydroxide and oxygen adsorption concentration. Diamond and circle symbols indicate oxygen adsorbed platinum component and platinum hydroxide component, respectively. The closed symbols are Pt–Co alloy catalysts and the open symbols are Pt nano-particle catalyst.

Beard et al. [16] detected less cobalt dissolution by annealing at 1200 °C than at 900 °C in Phosphoric Acid Fuel Cell operation. High temperature annealing may induce the segregation and stabilize the surface platinum ordering and bonding.

In order to investigate the mechanism of platinum dissolution from Pt–Co alloy catalysts, we measured Pt 4*f* core levels by SXPES. Pt 4*f* spectral changes in all the catalysts under initial MEA and cycle-tested MEA conditions are compared in Fig. 4. The binding energy of all spectra is collected by the rising part of the Pt $4f_{7/2}$ peak. The shapes of all the spectra are similar to the reference platinum foil, indicating that platinum in MEA exists mainly in the metallic form.

The measured spectra are fitted with Voigt (Gaussian and Lorentzian) functions and are deconvoluted into Pt^0, PtO_{ads}, $Pt(OH)_2$, PtO and PtO_2 [17–22] as shown in Fig. S2 of the supporting material. Reports on the assignment of PtO_{ads} and $Pt(OH)_2$ are limited

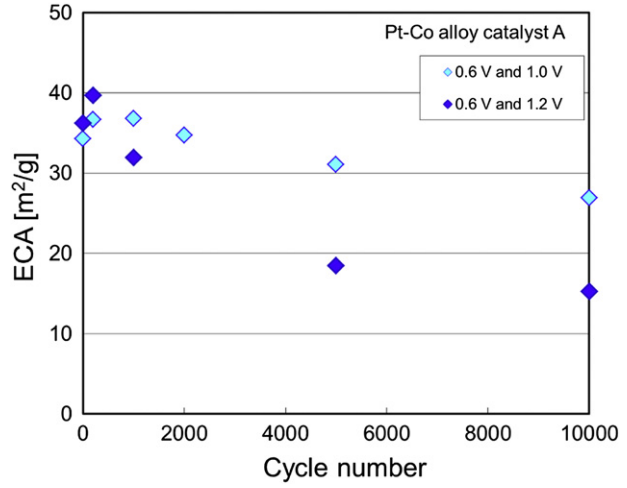

Fig. 7. Upper potential dependence of the ECA decay. ECA tested between 0.6 V and 1.2 V indicated by dark color symbols is compared with ECA tested between 0.6 V and 1.0 V by light color symbols, which is the same data as shown in Fig. 1. (For interpretation of the references to colour in this figure legend, the reader is referred to the web version of this article.)

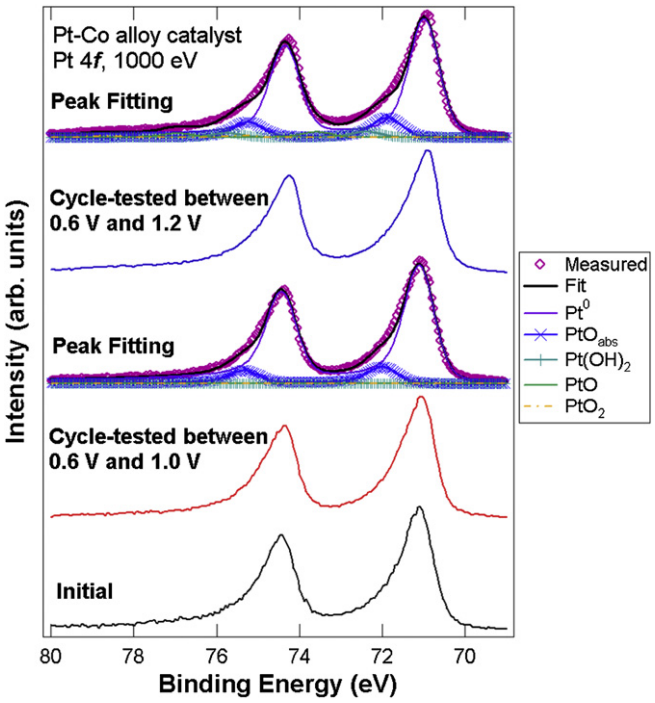

Fig. 8. Pt 4*f* core-level SXPES spectra for cycle-tested catalysts with upper potentials of 1.0 V and 1.2 V. Thin line is for 1.0 V, and solid line is for 1.2 V. The catalyst A is used for both MEAs.

compared to the assignment of Pt oxides. Miller et al. [22] measured Pt 4*f* XPS spectra introducing low pressure oxygen gas and assigned the peak between 71.6 and 71.7 eV as '4O', which corresponds to PtO_{ads} in this work. Wakisaka et al. [23] measured O 1*s* spectra of Pt–Fe alloy cathode catalysts using XPS, which is connected to a chamber with an electrochemical cell, in order to investigate the oxygen species on the catalysts in the electrochemical cell. They confirmed adsorption of OH species on the catalysts under the potential cycling between 0.8 and 1.0 V. Imai et al. [24] confirmed the presence of Pt–OH bonding in the same potential range using in-situ XAFS measurement. Since our MEA samples were tested introducing humidified gases, the catalyst layer should contain water in the presence of hydrophilic ionomer around the catalysts. The concentration of each chemical component obtained from the peak fitting is listed in Table 2. Since the concentration of platinum oxides (PtO and PtO_2) for all the catalysts is quite small, contribution of the platinum oxides to the catalyst degradation cannot be discussed. In order to identify chemical species of platinum that induce platinum dissolution, ECA decay rates are plotted against $Pt(OH)_2$ and PtO_{ads} concentrations of the initial MEA in Fig. 5. The ECA decay rate increased with the $Pt(OH)_2$ concentration. Because the $Pt(OH)_2$ concentration in the initial phase corresponds to the degree of platinum oxidation, it is natural to think that the $Pt(OH)_2$ concentration might have a correlation with oxidative tendency

Table 3
Chemical states composition in 1.0 V and 1.2 V obtained from SXPES measurement (%).

		Pt^0	PtO_{ads}	$Pt(OH)_2$	PtO	PtO_2
Peak shift from Pt^0 (eV)		0	0.9 [17,22]	1.4 [18]	2.6 [17,21]	4.4 [17]
0.6 V and 1.0 V	Initial	86	12	2	1	0
	Cycle-tested	87	13	0	0	0
0.6 V and 1.2 V	Cycle-tested	78	13	4	4	1

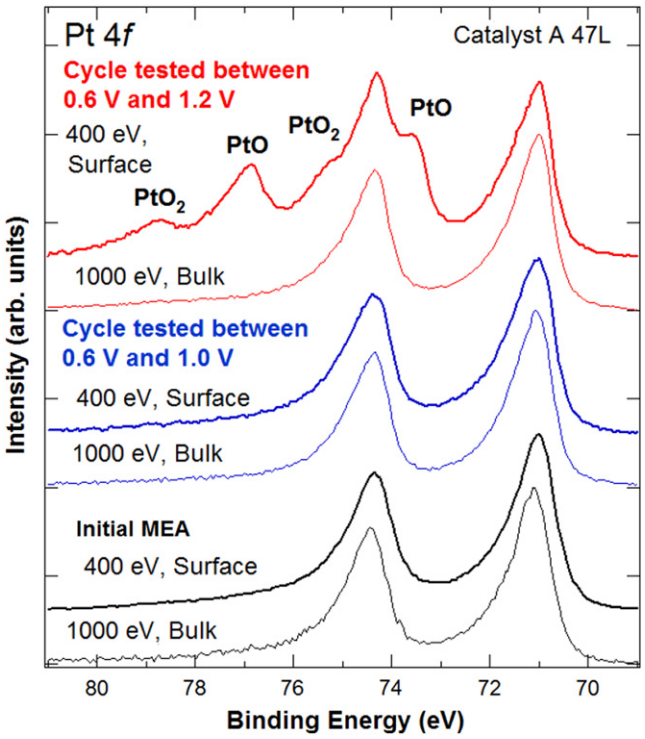

Fig. 9. Pt 4*f* core-level SXPES spectra at 400 eV excitation (thick lines) and 1 keV excitation (thin lines) for the initial MEA and the cycle-tested MEA with upper potentials of 1.0 V and 1.2 V.

during the potential cycling. On the other hand, the ECA decay rate is independent of PtO_{ads}. Thus it is found that the adsorbed oxygen species does not induce the ECA decay. Since the sum of metallic platinum and oxygen adsorbed platinum was slightly increased after the potential cycling, dissolved $Pt(OH)_2$ might be deposited on other platinum particles in reduction potential as a metallic state, Pt^0, and/or oxygen adsorbed platinum, PtO_{ads}.

We have measured the Pt 4*f* spectra of Pt nano-particle catalyst before and after potential cycling [12]. The ECA decay ratio after the potential cycling against the concentration of PtO_{ads} and $Pt(OH)_2$ is compared in Fig. 6. Since the ECA decay of the Pt nano-particle catalyst is not linear to the number of the potential cycling, we plot the ECA decay ratio after the potential cycle. Our previous results on Pt nano-particle catalyst are plotted in the figure as open symbols. The concentration of PtO_{ads} and $Pt(OH)_2$ of Pt nano-particle catalysts is larger than that of Pt–Co alloy catalysts. The ECA decay ratio increased linearly with the concentration of $Pt(OH)_2$. Fig. 6 indicates that the Pt dissolution for Pt nano-particle catalyst and Pt–Co alloy catalysts occurred in the same mechanism.

3.2. Potential effect on catalyst degradation

In order to investigate the oxidation effect on catalyst durability, we conducted the potential cycling on the catalyst A 47L with higher upper potential, 1.2 V. As shown in Fig. 7, the ECA decay for the potential cycling between 0.6 V and 1.2 V was larger than that for the potential cycling between 0.6 V and 1.0 V. The results suggest that a larger amount of platinum should dissolve at 1.2 V than at 1.0 V and may accelerate the catalyst degradation. In order to observe platinum oxidation induced by the higher upper potential, the Pt 4*f* spectra after potential cycling with upper potential of 1.2 V are compared with those with 1.0 V in Fig. 8. The Pt 4*f* peaks after potential cycling with upper potential of 1.2 V are slightly broadened to higher binding energy side than that with 1.0 V. Platinum components extracted from the peak fitting in Fig. 8 are listed in Table 3. It is found from Tables 2and 3 that after the potential cycling between 0.6 V and 1.0 V, platinum oxides, PtO and PtO_2, do not exist, while several percentages of platinum oxides appear after the potential cycling between 0.6 V and 1.2 V. Thus PtO and PtO_2 may be produced at the 1.2 V step. Imai et al. [24] have reported that the platinum oxidation depends on the cell potential and the platinum oxide PtO and PtO_2 formed over 1.08 V. In order to confirm the existence of the platinum oxide on the surface of the catalyst particles, PES spectra with 400 eV for photon energy, which is more surface sensitive for Pt 4*f* core levels than 1 keV excitation, were obtained. The probing depths are 1.7 nm with 400 eV and 3.4 nm with1 keV, respectively. The Pt 4*f* spectra are compared between 400 eV and 1 keV in Fig. 9 for the initial MEA, the cycle-tested MEA with upper potential of 1.0 V and the cycle-tested MEA with upper potential of 1.2 V. On the cycle-tested MEA with upper potential of 1.2 V, PtO peaks appeared at 73.5 eV and 76.9 eV and the PtO_2 peaks appeared at 75.3 eV and 78.7 eV as labeled in Fig. 9. Thus, it is confirmed that the platinum oxides formed on the surface of the catalyst particles in the potential cycling with upper potential of 1.2 V.

From our results the potential cycling with the upper potential of 1.2 V produces platinum oxides and accelerated the catalyst degradation by the dissolution of the platinum oxides from the catalysts.

4. Conclusion

Platinum oxidation of four types of Pt–Co alloy catalysts for polymer electrolyte fuel cells was investigated by soft X-ray photoemission spectroscopy to elucidate the origin of catalyst degradation. The ECA decreased more slowly in the catalysts with larger particle size and in those with higher annealing temperature. It is found that the concentration of platinum hydroxide, $Pt(OH)_2$, is related to the catalyst degradation during the potential cycling between 0.6 and 1.0 V, while the oxygen adsorbed platinum does not seem to affect the catalyst degradation. The oxygen adsorption might be too weak to break the Pt–Pt bonding to cause Pt dissolution from the catalyst particles. Applying potential cycling up to 1.2 V, platinum oxides, PtO and PtO_2, appeared and the catalyst degradation was more accelerated than the potential cycling up to 1.0 V. Thus the platinum oxides produced during potential cycling up to 1.2 V should also contribute to the catalyst degradation. These platinum hydroxide and platinum oxides seem to induce the catalyst degradation by being dissolved from the catalyst particles. Our results suggest that preventing the platinum oxidation on the surface of the catalyst by optimizing the catalyst particle size and the annealing temperature can be one of the solutions to improve the catalyst durability.

Acknowledgments

This work was supported by New Energy and Industrial Technology Development Organization (NEDO). The XPS experiments were approved by the Japan Synchrotron Radiation Research Institute (JASRI) Proposal Review Committee (Proposal No. 2009A1617 and 2011A1538). The authors would like to thank Dr. Muro and Dr. Izumi for the technical supports on SXPES measurements at SPring-8.

Appendix A. Supplementary material

Supplementary material associated with this article can be found, in the online version, at doi:10.1016/j.jpowsour.2012.05.001.

References

[1] H.A. Gasteiger, S.S. Kocha, B. Sompalli, F.T. Wagner, Appl. Catal. B: Environ. 56 (2005) 9–35.
[2] V. Stamenkovic, B.S. Mun, K.J.J. Mayrhofer, P.N. Ross, N.M. Markovic, J. Rossmeisl, J. Greeley, J.K. Norskov, Angew. Chem. Int. Ed. 45 (2006) 2897–2901.
[3] V.R. Stamenkovic, B.S. Mun, M. Arenz, K.J.J. Mayrhofer, C.A. Lucas, G. Wang, P.N. Ross, N.M. Markovic, Nat. Mater. 6 (2007) 241–247.
[4] T. Toda, H. Igarashi, H. Uchida, M. Watanabe, J. Electrochem. Soc. 146 (1999) 3750–3756.
[5] M.S. Wilson, F.H. Garzon, K.E. Sickafus, S. Gottesfeld, J. Electrochem. Soc. 140 (1993) 2872–2877.
[6] P.J. Ferreira, G.J. la O', Y. Shao-Horn, D. Morgan, R. Makharia, S. Kocha, H.A. Gasteiger, J. Electrochem. Soc. 152 (2005) A2256–A2271.
[7] Y. Shao-Horn, W.C. Sheng, S. Chen, P.J. Ferreira, E.F. Holby, D. Morgan, Top. Catal. 46 (2007) 285–305.
[8] S. Mitsushima, S. Kawahara, K. Ota, N. Kamiya, J. Electrochem. Soc. 154 (2007) B153–B158.
[9] P. Yu, M. Pemberton, P. Plasse, J. Power Sources 144 (2005) 11–20.
[10] S. Chen, H.A. Gasteiger, K. Hayakawa, T. Tada, Y. Shao-Horn, J. Electrochem. Soc. 157 (2010) A82–A97.
[11] K. Matsutani, K. Hayakawa, T. Tada, Platinum Metals Rev. 54 (2010) 223–232.
[12] S. Hidai, M. Kobayashi, H. Niwa, Y. Harada, M. Oshima, Y. Nakamori, T. Aoki, J. Power Sources 196 (2011) 8340–8345.
[13] L.M. Roen, C.H. Paik, T.D. Jarvi, Electrochem. Solid-State Lett. A19 (2004) A19–A22.
[14] T. Kinumoto, K. Takai, Y. Iriyama, T. Abe, M. Inaba, Z. Ogumi, J. Electrochem. Soc. 153 (2006) A58–A63.
[15] T.R. Ralph, G.A. Hards, J.E. Keating, S.A. Campbell, D.P. Wilkinson, M. Davis, J. St-Pierre, M.C. Johnson, J. Electrochem. Soc. 144 (1997) 3845–3857.
[16] B.C. Beard, P.N. Ross Jr., J. Electrochem. Soc. 137 (1990) 3368–3374.
[17] K.S. Kim, N. Winograd, R.E. Davis, J. Am. Chem. Soc. 93 (1971) 6296–6297.
[18] J.S. Hammond, N. Winograd, J. Electroanal. Chem. 78 (1977) 55–69.
[19] M.C. Jung, H.D. Kim, M. Han, W. Jo, D.C. Kim, Jpn. J. Appl. Phys. 38 (1999) 4872–4875.
[20] C.R. Parkinson, M. Walker, C.F. McConville, Surf. Sci. 545 (2003) 19–33.
[21] R. Liu, H. Iddir, Q. Fan, G. Hou, A. Bo, K.L. Ley, E.S. Smotkin, Y.E. Sung, H. Kim, S. Thomas, A. Wieckowski, J. Phys. Chem. B 104 (2000) 3518–3531.
[22] D.J. Miller, H. Oberg, S. Kaya, H.S. Casalongue, D. Friebel, T. Anniyev, H. Ogasawara, H. Bluhm, L.G.M. Pettersson, A. Nilsson, Phys. Rev. Lett. 107 (2011) 195502.
[23] M. Wakisaka, H. Suzuki, S. Mitsui, H. Uchida, M. Watanabe, J. Phys. Chem. C 112 (2008) 2750–2755.
[24] H. Imai, K. Izumi, M. Matsumoto, Y. Kudo, K. Kato, Y. Imai, J. Am. Chem. Soc. 131 (2009) 6293–6300.